Test Samples for the Hayabusa Sample-Return Mission: Mineralogy and Petrology

By

Kazushige TOMEOKA[1], Ichiro OHNISHI[1], Naotaka TOMIOKA[1], Mitsuhiro SUGITA[1] and Kouji ADACHI[2]

Abstract: We have studied the mineralogy and petrology of the Hayabusa test samples, 3A and 3B, using an optical microscope, a scanning electron microscope (SEM) and an electron probe micro-analyzer. We also used an analytical field emission SEM and an analytical transmission electron microscope to obtain information especially at high magnification. The 3A sample is powder composed of particles (<150 μm in diameter) that consist mainly of fine grains of Fe-rich olivine, low-Ca pyroxene and lesser amounts of high-Ca pyroxene and plagioclase. The 3B sample is composed of rounded to subrounded particles (0.2-2.3 mm in diameter) that consist mainly of Fe-Ni metal and lesser amounts of Fe-rich olivine and low-Ca pyroxene. Both 3A and 3B particles contain materials that are analogous in texture to chondrules in chondrites. Fe-rich olivine and low-Ca pyroxene in both 3A and 3B are highly homogeneous in composition. Although the general appearance and the relative abundances of constituent minerals are different between 3A and 3B, most constituent minerals occur in common and have very similar compositions that closely resemble those of the counterparts in equilibrated H ordinary chondrites. The results suggest that 3A is made of a silicate-rich fraction of an equilibrated H chondrite and 3B is made of a metal-rich fraction of an equilibrated H chondrite. 3B particles may correspond to individual silicate-bearing metal grains in an H chondrite. Although precise determination of petrologic type is difficult because of very small particle size, we suggest that the petrologic type of both 3A and 3B is relatively low.

1. INTRODUCTION

Hayabusa is the first sample-return mission to an asteroid in the human history, and thus the outcome of this mission is awaited with great expectation. The target asteroid 25143 Itokawa made its close approach to Earth in 2001, and during that time, extensive ground-based telescopic observations were made to characterize its physical and chemical properties in preparation for the mission. Visible and near-infrared spectroscopic measurements (Binzel et al., 2001) reveal that the surface material of Itokawa has a red-slope S-type spectrum analogous to those measured for LL ordinary chondrites. Photometric measurements (Lederer et al., 2005) indicate that Itokawa appears to be a space-weathered, atypical S-class asteroid. Although much still remains to be known, these results suggest that Itokawa may be related to the primitive chondrite meteorites.

Our group in Kobe University has long been involved in research on chondrite meteorites and interplanetary dust particles (IDPs). These materials consist largely of extremely small mineral grains, most of which are submicrometer in size. Thus, to study them we have used a combination of various techniques capable of viewing and analyzing ultra-microscopic particles.The sample that will be collected from Itokawa is regarded to be very small in amount and consist of very small particles. We believe that our expertise and experience that we have gained through the studies of the fine-grained meteorites and IDPs would contribute to the study of the sample returned from Itokawa.

1 Department of Earth and Planetary Sciences, Faculty of Science, Kobe University, 1-1 Rokkoudai-cho, Nada, Kobe 657-8501, JAPAN

2 Graduate School of Science and Technology, Kobe University, 3-11 Tsurukabuto, Nada, Kobe 657-8501, JAPAN

We have received two test samples, termed 3A and 3B (each weighs～100 mg), from ISAS/JAXA on December 7, 2004. Both samples are composed of very small particles that themselves consist of fine grains of various minerals. In this paper, we present the results of petrographic and electron microscopic studies of these two test samples. The objective of our study is to provide mineralogical and petrological details of the test samples, and thereby to demonstrate our capability of characterizing small particles. We assumed that the test samples were probably prepared from meteorites. Thus, we also intend to determine their meteoritic classification as precisely as possible.

2. MATERIALS AND METHODS

2.1. Samples

The 3A sample (～100 mg) is dark grayish powder that consists of angular to irregularly shaped particles ranging in diameter from 10 to 150 μm (Fig. 1a). Four powder samples, each weighs 0.5-1.5 mg (～5 mg in total), were scooped up from the 3A sample and used for the following investigation. Initially one sample was observed by a field emission scanning electron microscope (FESEM) to study morphology and surface mineralogy of particles. Other two samples were embedded in an epoxy resin on glass slides, and polished sections of powder particles were made of them. The last sample was ground by an agate mortar to make finer-grained powder for transmission electron microscope (TEM) investigation. A small droplet of ethanol, in which the powder was suspended, was dried on a TEM grid that is reinforced with a thin carbon film.

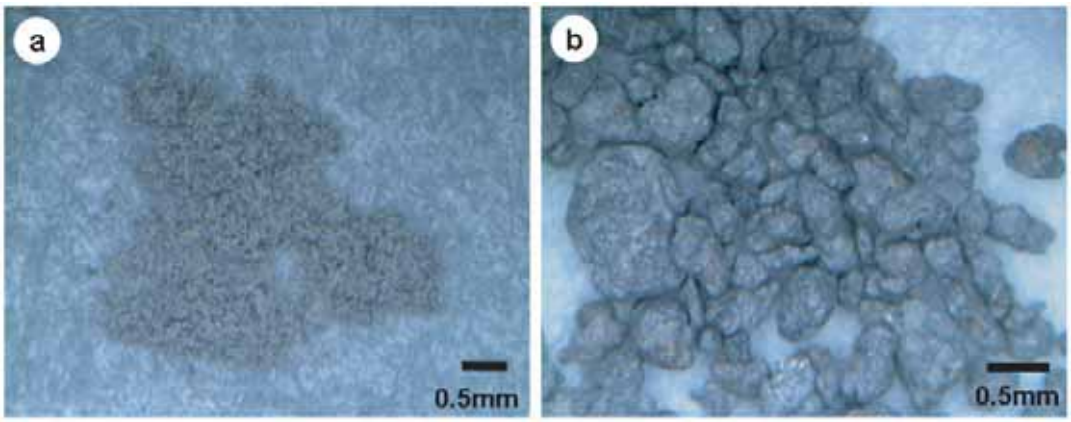

Figure 1. Optical micrographs of the 3A sample (a) and the 3B sample (b).

Table 1. Diameters and areas of 3B particles and modal abundances of Fe-Ni metal measured on the sections.

Particle name	Particle diameter* (mm)	Particle area (mm^2)	Metal area (%)
3B-1	2.3	3.41	42
3B-2	1.6	1.77	46
3B-3	0.8	0.37	48
3B-4	1.3	1.12	44
3B-5	1.0	0.60	55
3B-6	1.3	1.00	61
3B-7	0.8	0.33	55
3B-8	0.5	0.12	72

*Average of two dimensions.

The 3B sample (～100 mg) consists of dark grayish, rounded to sub-rounded particles that range in diameter from 0.2 to 2.3 mm (Fig. 1b). They are commonly elongated and uneven on the surfaces, exhibiting a peculiar, potato-like external shape. Most particles partly have metallic luster. Two largest particles (～2.3 and ～1.6 mm in diameter) and six relatively large particles (0.5-1.3 mm), termed 3B-1 to 3B-8, were hand-picked under an optical stereo-microscope for the following investigation (Table 1); the total amount of the particles is ～39 mg. Polished thin and thick sections were made from those eight particles. 3B was not studied by the TEM, because grain sizes of most minerals in 3B are much larger than those in 3A, and thus, most of mineralogical data could be obtained by the SEM and EPMA.

2.2. Analytical Methods

Polished thin and thick sections were studied using an optical microscope, a scanning electron microscope (SEM) (JEOL JSM-6480) and a field emission scanning electron microscope (FESEM) (JEOL JSM-6330F), both equipped with energy dispersive X-ray spectrometers (EDS), and an electron probe micro-analyzer (EPMA) (JEOL JXA-8900) equipped with wavelength-dispersive X-ray spectrometers (WDS). EDS analyses with the SEM were obtained at 15 kV and 0.4 nA, those with the FESEM at 15 kV and 0.3 nA, and WDS analyses at 15 kV and 12 nA. Data corrections were made by the Phi-Rho-Z method for EDS analyses. For WDS analyses of silicates and oxides, data corrections were made by the Bence-Albee method. For WDS analyses of metals and sulfides, data corrections were made by the ZAF method. For WDS analyses of metals, special care was taken to determine Co contents; Co background counts were taken at wavelengths of 0.177 nm and 0.183 nm to eliminate the contribution of the Fe K_β peak to the Co K_α peak (Rubin, 1990; Shibata, 1996). Well-characterized natural and synthetic minerals and glasses were used as standards. For most SEM and FESEM observations, we used backscattered electron (BSE) imaging. For the analysis of each mineral grain, we used a focused electron beam of ～2 μm in diameter.

Imaging and electron diffraction were performed with a transmission electron microscope (TEM) (JEOL JEM-2010) equipped with EDS, operated at 200 kV. Identification of crystal structure was based on selected-area electron diffraction (SEAD) and high-resolution imaging.

The modal analysis of metal was performed by using an image processing method. Digitized backscattered electron images were converted, using the Adobe Photoshop software package, to a histogram showing a brightness distribution of individual pixels in the images. Metal shows the highest brightness among the constituent minerals in the samples. After determining a proper threshold level in the histogram, a 255 level black and white image was converted to a straight black and white (0/255) image, and modal% of metal was calculated as an area percentage of white spaces (which correspond to metal) to a whole image.

3. RESULTS ON 3A SAMPLE

3.1. Petrography and Mineralogy

SEM observations of the polished sections of the particles reveal that they consist mainly of fine grains (5-150 μm in size) of olivine, low-Ca pyroxene, and lesser amounts of high-Ca pyroxene and plagioclase (Figs. 2a, b). Minor minerals include Fe-Ni metal, troilite, Ca-phosphate and chromite. In most particles, olivine and pyroxene occur as porous aggregates of very fine grains (5-20 μm) that are angular to irregular in shape and commonly have fine fractures and voids at high density (Fig. 2b). Fe-Ni metal, mostly kamacite with minor taenite, and troilite comprise <10 vol%; they occur as grains 5-50 μm in size. Particles that consist entirely of a single mineral of Fe-Ni metal or troilite occur in minor proportions. Neither hydrous minerals such as phyllosilicates nor Ca-Al-rich inclusion-like materials have been observed.

Some particles have textures similar to the interior of chondrules in chondrites (Figs. 3a-d), although no whole chondrules have been observed. The textural types include porphyritic olivine (PO), porphyritic pyroxene (PP) and barred olivine (BO). Plagioclase fills interstices between olivine and pyroxene grains and commonly has fine, acicular to lath-shaped crystallites (0.2-2 μm in width, 1-30 μm in length) of high-Ca pyroxene, mostly diopside (Fig. 3d), exhibiting an appearance similar to chondrule mesostasis. Because of small grain size and large sample thickness, we could not optically confirm the presence of isotropic glass in the

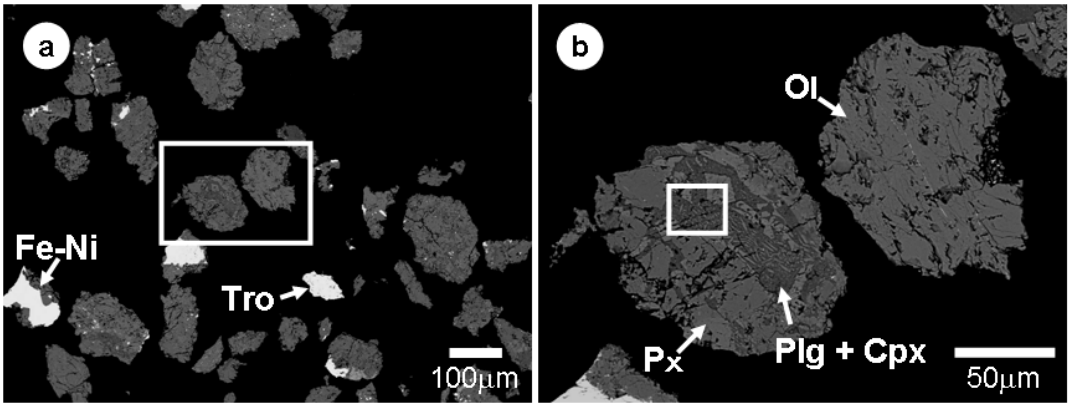

Figure 2. (a) Backscattered electron image of a polished section of 3A particles. (b) Image of boxed area in (a). Fe-Ni = Fe-Ni metal, Tro = troilite, Ol = olivine, Px = low-Ca pyroxene, Cpx = high-Ca pyroxene, Plg = plagioclase.

mesostasis. FESEM observations reveal that plagioclase in some particles has numerous submicron-size vesicles and spherical inclusions (<1-5 μm in diameter) of troilite and Fe-Ni metal as well as minor amounts of chromite and ilmenite (Figs. 4a, b).

Transmission electron microscope (TEM) observations of a powdered sample confirm the presence of most minerals described above. Olivine grains have very low densities of dislocations. Selected-area electron diffraction (SAED) patterns of low-Ca pyroxene grains show that they are mostly monoclinic clino-pyroxene with minor stacking faults on (100) plane (Figs. 5a, b). SEAD patterns of Na-Al-Si-O-rich grains show that they are mostly crystalline plagioclase but some are glassy; because of limited number of grains observed, relative abundance of crystalline and glassy phase is not clear.

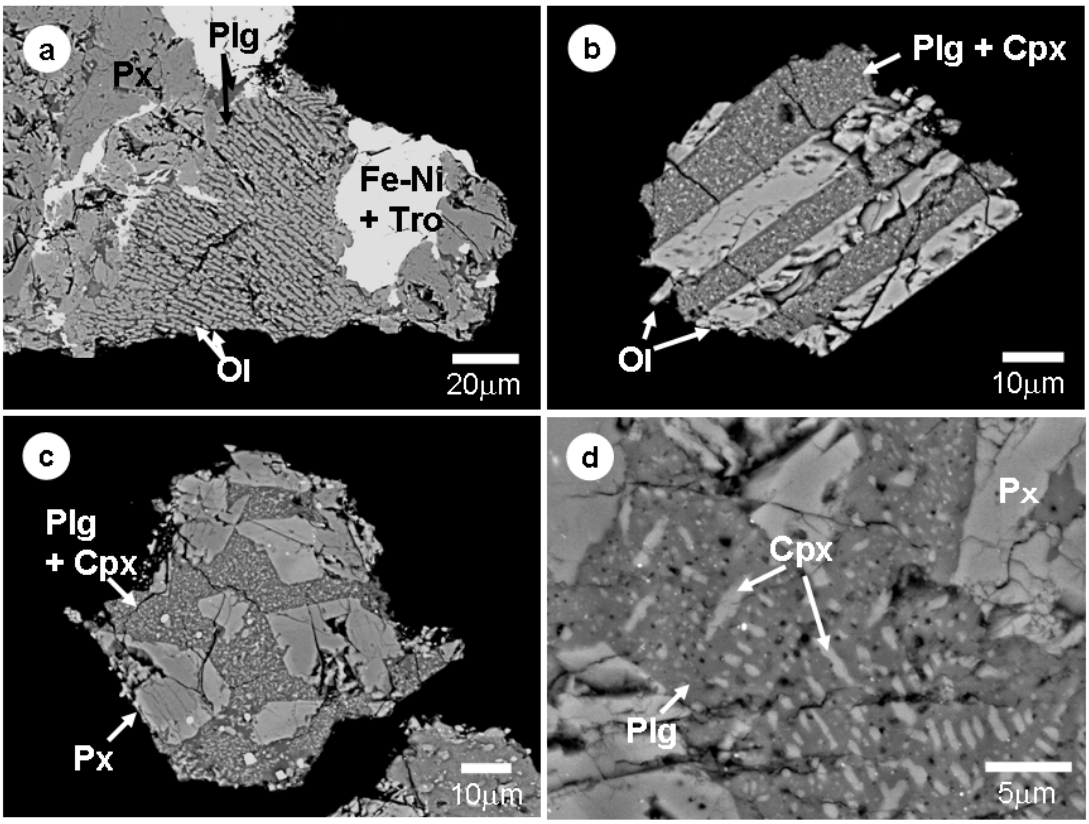

Figure 3. Backscattered electron images of 3A particles showing textures similar to the interior of chondrules in chondrites. (a, b) Barred olivine type. (c) Porphyritic pyroxene type.(d) High-magnification image of boxed area in Fig. 2b, obtained using the field emission SEM, showing quenched crystallites of high-Ca pyroxene (Cpx) in plagioclase (Plg) mesostasis. Fe-Ni = Fe-Ni metal, Tro = troilite, Ol = olivine, Px = low-Ca pyroxene.

3.2. Mineral Compositions

Olivine is very homogeneous, averaging $Fa_{15.8}$ (standard deviation in Fa content = 0.6) (Table 2; Fig. 6). It contains significant amounts of Mn (～0.5 wt% MnO) and extremely low amounts of Ca (<0.05 wt% CaO), Ti (<0.05 w% TiO_2) and Cr (<0.05wt% Cr_2O_3).

Low-Ca pyroxene is also very homogeneous, averaging $Fs_{14.2}$ (standard deviation in Fs content=1.0) (Fig. 7) and $Wo_{0.9}$ (Table 2; Fig. 8). It contains significant amounts of Al (～0.2 wt% Al_2O_3), Cr (～0.2 wt% Cr_2O_3) and Mn (～0.5 wt% MnO). High-Ca pyroxene is also homogeneous in Fs content, averaging $Fs_{6.4}$ (standard deviation in Fs content = 0.9) and $Wo_{40.2}$ (Table 2), but shows slight variations in Ca content (standard deviation in Wo content = 4.1) (Fig. 8). High-Ca pyroxene contains significant amounts of Na (～0.7 wt% Na_2O), Al (～1.5 wt% Al_2O_3), Ti (～0.5 wt% TiO_2), Cr (～1.5 wt% Cr_2O_3) and Mn (～0.3 wt% MnO).

Plagioclase is albitic (Na-rich). In contrast to olivine and pyroxene, it is variable in composition from grain to grain, ranging from An_{12} to An_{33} (Table 2; Fig. 9).

Kamacite contains ～5.5 wt% Ni and ～0.45 wt% Co (Table 3). Taenite contains ～33.0 wt% Ni and trace amounts of Co (～0.07 wt%). Ni contents in taenite show considerable variation (28-40 wt% Ni) from grain to grain.

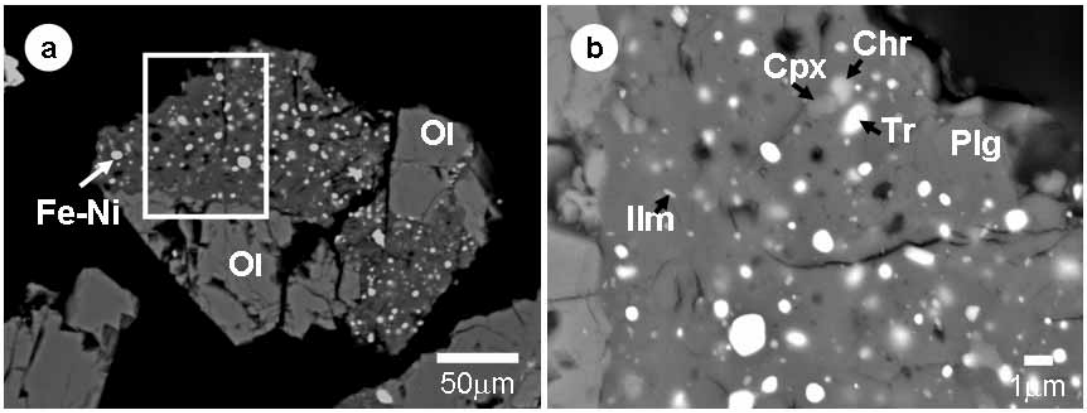

Figure 4. (a) Backscattered electron image of a 3A particle that contains numerous submicron-size spherical inclusions and vesicles in plagioclase (Plg). (b) High-magnification image of boxed area in (a), obtained using the field emission SEM, showing inclusions of high-Ca pyroxene (Cpx), ilmenite (Ilm), chromite (Chr), and troilite (Tro) grains and vesicles (dark in contrast) in plagioclase. Fe-Ni = Fe-Ni metal, Ol = olivine, Px = low-Ca pyroxene.

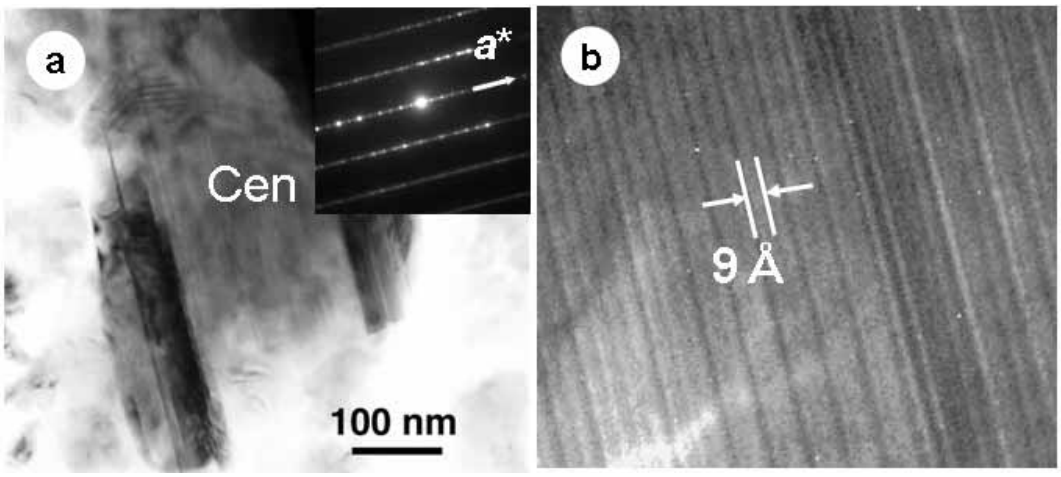

Figure 5. (a) TEM image of a low-Ca pyroxene (clino-enstatite: Cen) grain in the 3A sample. The selected-area electron diffraction (SAED) pattern from this grain (inset) shows diffuse streaks along a^* with intensity maxima corresponding to clino-enstatite. (b) High-resolution TEM image of the grain in (a) showing irregularities produced by stacking faults between ortho- and clino-enstatite.

Table 2. Electron microprobe analyses of olivine, low-Ca pyroxene, high-Ca pyroxene and plagioclase in the 3A sample (wt%).

	Olivine		Low-Ca pyroxene		High-Ca pyroxene		Plagioclase	
No. of Analyses	33	s.d.	45	s.d.	5	(s.d.)	9	(s.d.)
Na_2O	0.01	(0.01)	0.02	(0.02)	0.73	(0.09)	8.61	(0.68)
MgO	45.1	(0.4)	32.5	(0.7)	18.6	(1.3)	0.33	(0.21)
Al_2O_3	0.01	(0.01)	0.19	(0.12)	1.48	(0.95)	22.9	(1.3)
SiO2	39.0	(0.4)	56.2	(0.5)	53.8	(0.6)	62.1	(2.1)
K_2O	0.00	(0.01)	0.01	(0.01)	0.01	(0.01)	0.26	(0.08
CaO	0.02	(0.02)	0.6	(0.28)	19.5	(1.9)	4.77	(1.37)
TiO_2	0.03	(0.04)	0.10	(0.08)	0.49	(0.31)	0.17	(0.13)
Cr_2O_3	0.02	(0.03)	0.18	(0.13)	1.53	(0.19)	0.29	(0.44)
MnO	0.45	(0.04)	0.48	(0.07)	0.34	0.03)	0.02	(0.02)
FeO	15.1	(0.6)	9.69	(0.65)	3.95	(0.53)	0.59	(0.28)
NiO	0.01	(0.02)	0.01	(0.02)	0.02	(0.03)	0.01	(0.01)
Total	99.8		99.9		100.4		100.0	
Mol%								
Fa	15.8	(0.6)	-	(-)	-	(-)	-	(-)
Fs	-	(-)	14.2	(1.0)	6.4	(0.9)	-	(-)
Wo	-	(-)	0.9	(0.5)	40.2	(4.1)	-	(-)
Ab	-	(-)	-	(-)	-	(-)	75.5	(6.1)
An	-	(-)	-	(-)	-	(-)	23.1	(6.5)
Or	-	(-)	-	(-)	-	(-)	1.5	(0.5)

s.d.: standard deviation.

Table 3. Electron microprobe analyses of kamacite, taenite and troilite in the 3A sample (wt%).

	Kamacite}		Taenite		Troilite	
No. of Analyses	27	(s.d.)	13	(s.d.)	11	(s.d.)
P	0.00	(0.00)	0.00	(0.00)	0.00	(0.00)
Si	0.01	(0.01)	0.01	(0.01)	0.01	(0.01)
S	0.00	(0.00)	0.02	(0.04)	36.9	(0.1)
Cr	0.01	(0.01)	0.01	(0.02)	0.01	(0.01)
Fe	93.8	(0.6)	66.2	(4.7)	62.8	(0.4)
Ni	5.46	(0.40)	33.0	(4.4)	0.04	(0.10)
Co	0.45	(0.01)	0.17	(0.08)	0.00	(0.00)
Total	99.8		99.4		99.8	

s.d.: standard deviation.

Because Ca-phosphate and chromite occur as very fine grains (<2 μm), it was difficult to obtain good quantitative analyses from them. Ca-phosphate contains Cl but no F, and thus is probably chlorapatite. Chromite contains considerable Al, Mg, appreciable Mn and Ti.

4. RESULTS ON 3B SAMPLE

4.1. Petrography and Mineralogy

4.1.1. General Petrography

Optical microscope and SEM observations of the thin sections indicate that they consist mainly of Fe-Ni metal and silicates (Figs. 10a, b). X-ray chemical mapping also enables us to visualize the distribution of metal and silicates in the particles (Figs.

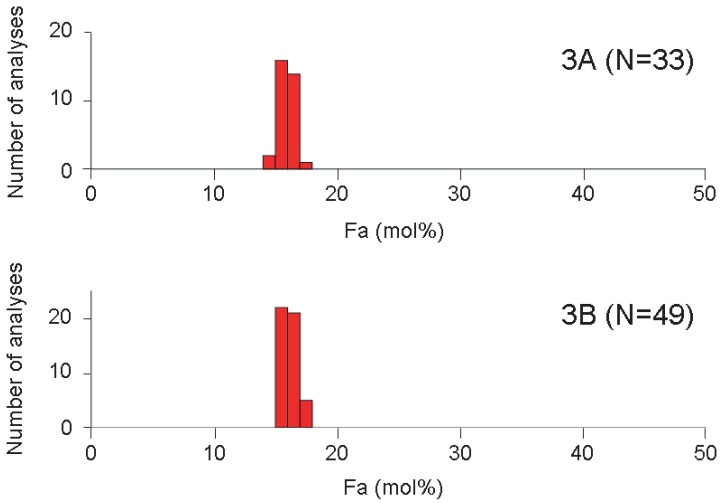

Figure 6. Fayalite concentrations in olivine in the 3A and 3B samples. Shown in the parentheses are number of analyses.

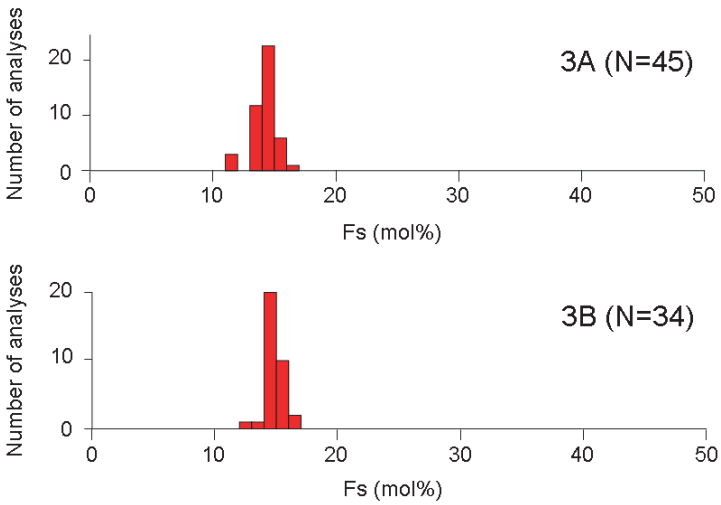

Figure 7. Ferrosilite concentrations in low-Ca pyroxene in the 3A and 3B samples. Shown in the parentheses are number of analyses.

11a-d). Fe-Ni metal fills interstices between silicate grains and is volumetrically the most abundant phase. The modal analysis indicates that metal comprises 42-72 vol% of each sample; the rest are mostly silicates (Table 1). Silicates are mainly olivine, low-Ca pyroxene and lesser amounts of high-Ca pyroxene and plagioclase. The silicates occur as rounded to subrounded aggregates (100 to 400 μm in diameter) and also as irregularly shaped aggregates (500-1000 μm) (Figs. 10a, b); the latter occur along the edge of individual particles and appear to be part of larger aggregates. Their external shape and internal texture suggest that they are chondrules and chondrule fragments. Olivine and low-Ca pyroxene also occur as single mineral fragments that are commonly rounded to subrounded in shape and range in diameter from 10 to 100 μm. Minor minerals are troilite, chromite and Ca-phosphate. Neither hydrous minerals nor Ca-Al-rich inclusion-like materials have been observed.

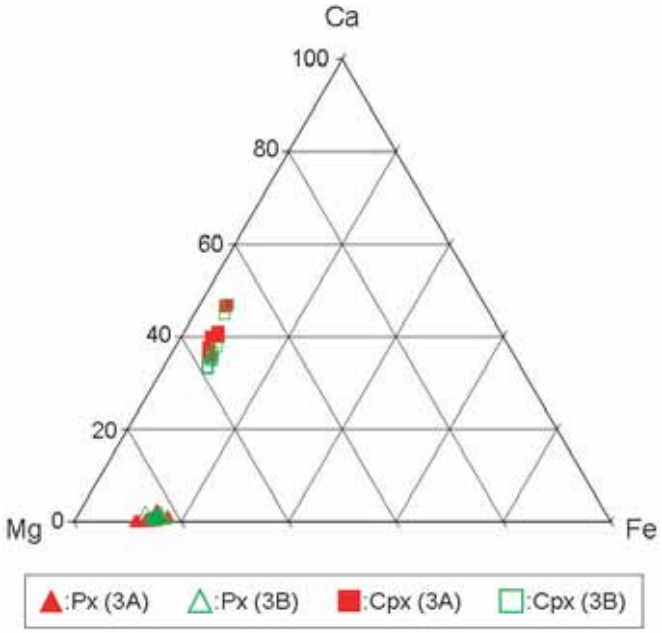

Figure 8. Analyses of low-Ca and high-Ca pyroxene in the 3A and 3B samples in terms of atomic percents of Ca, Mg, and Fe.Px = low-Ca pyroxene, Cpx = high-Ca pyroxene.

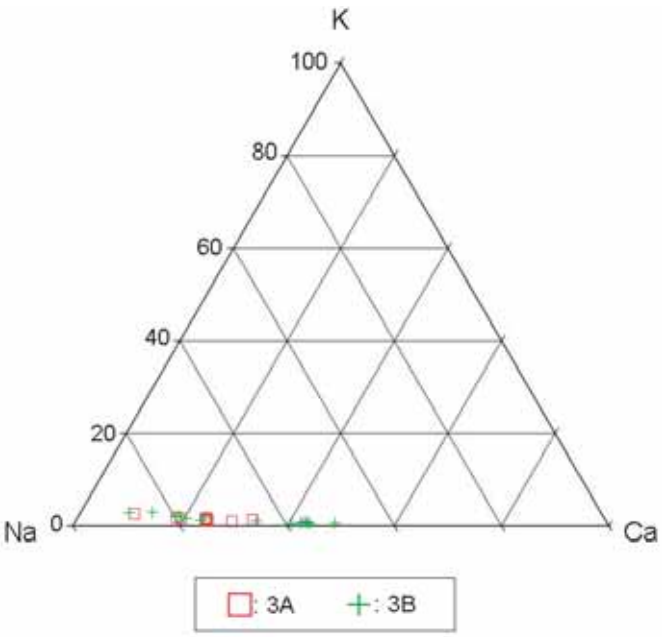

Figure 9. Analyses of plagioclase in the 3A and 3B samples in terms of atomic percents of K, Na, and Ca.

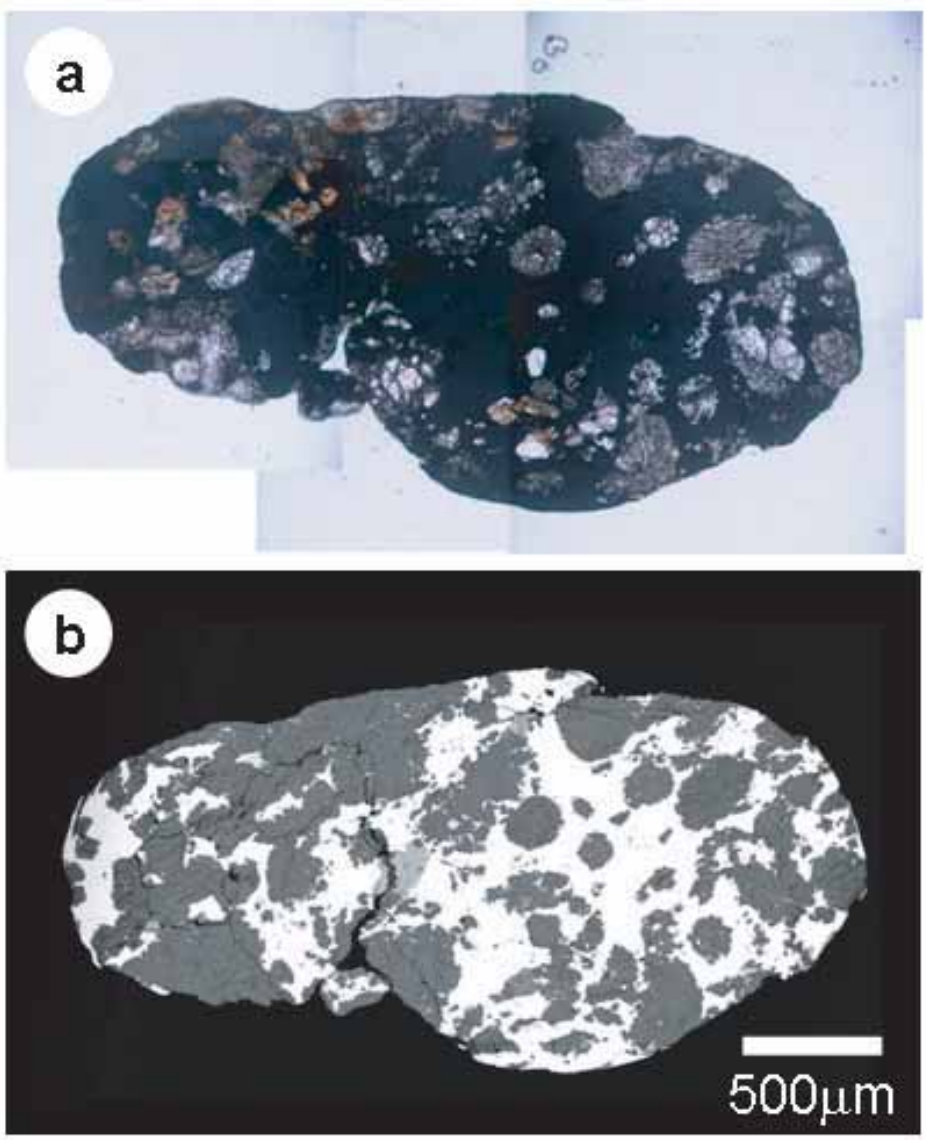

Figure 10. (a) Transmitted, plane-polarized light image of a thin section of the largest particle in the 3B sample. (b) Backscattered electron image of the same particle. The grayish areas consist of silicates, whereas the whitish areas consist of Fe-Ni metals.Note that the particle contains many chondrule-like silicate aggregates.

4.1.2. Silicate Aggregates

Silicate aggregates have porphyritic olivine (PO), porphyritic olivine-pyroxene (POP), and barred olivine (BO) type textures (Figs. 12a-d); other minor textural types include granular olivine (GO) and porphyritic pyroxene (PP). Olivine and low-Ca pyroxene occur as phenocrysts that range in size from 5 to 50 μm. Mesostases are filled with a material that is compositionally consistent with plagioclase; because of small grain size, it was difficult to optically confirm the presence of glass in the mesostasis; thus we call the mesostasis phase plagioclase. The plagioclase commonly contains fine, acicular to lath-shaped quenched crystallites (1-2 μm in width and 5-30 μm in length) of high-Ca pyroxene, mostly diopside (Fig. 12d). In places, it contains numerous vesicles (<2 μm in diameter) and micro-inclusions (<2 μm in diameter) of chromite and ilmenite. Troilite occurs as grains 1-20 μm in diameter; its abundance is much less than in 3A. Ca-phosphate occurs as irregularly shaped grains 20-100 μm in size. Although the silicate aggregates have a close resemblance to chondrules, no fine-grained matrix-like material has been found.

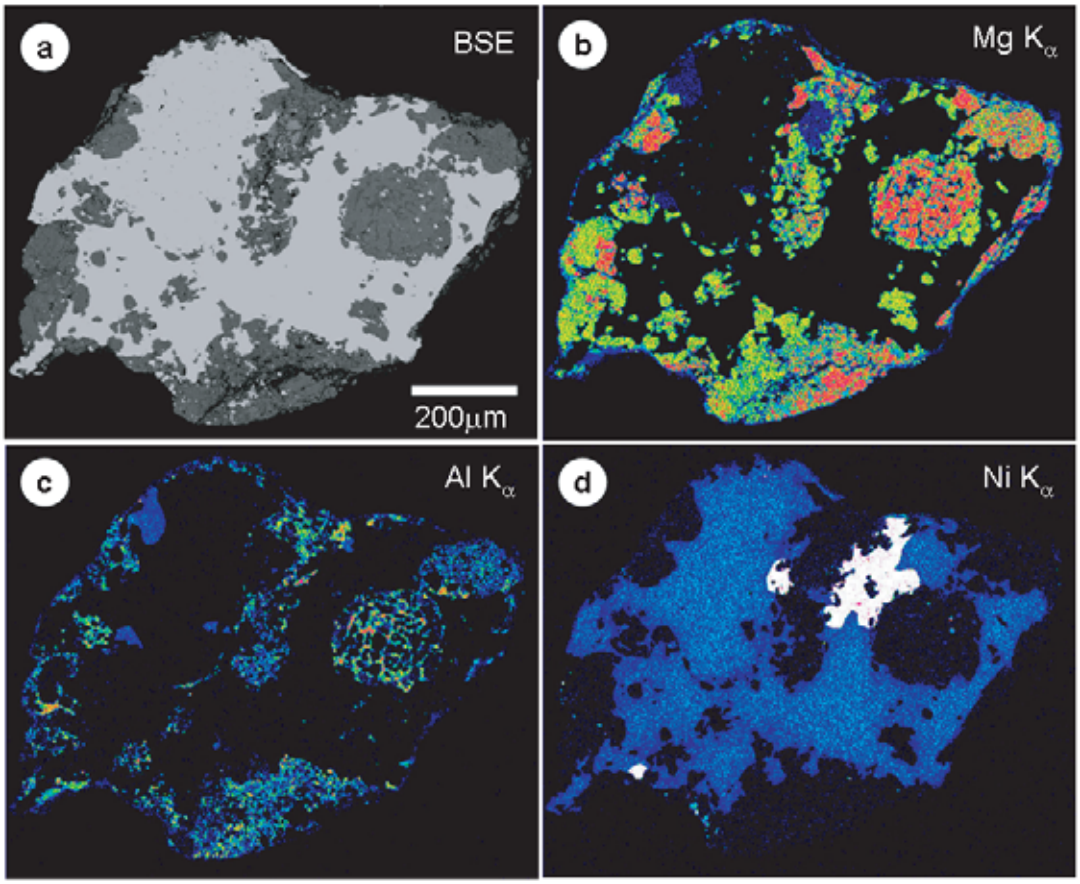

Figure 11. Backscattered electron image (a) and X-ray chemical maps of Mg K_α (b), Al K_α (c) and Ni K_α (d) of a 3B particle. In the X-ray chemical maps, the brighter an area is, the higher the concentration of an element is.Mg concentrations in (b) correspond to olivine and low-Ca and high-Ca pyroxene, Al concentrations in (c) to plagioclase, high-Ca pyroxene and chromite, and Ni concentrations in (d) to kamacite and taenite (bright grains). The map of Ni K_α (d) shows that kamacite grains exhibit compositional zoning, with a core of Ni-rich kamacite surrounded by a rim of more Ni-poor kamacite.

4.1.3. Metals

The predominant metal is kamacite. Minor amounts of taenite coexist with kamacite as grains ranging in size from 50 to 200 μm. Low-contrast BSE imaging reveals that kamacite shows a lamellae texture that consists of parallel oriented bands (1-10 μm in width) of Ni-poor kamacite in Ni-rich kamacite. X-ray chemical mapping shows that kamacite grains exhibit compositional zoning, with higher Ni contents in their cores than at their edges (Fig. 11d). Taenite grains also exhibit compositional zoning, with a core of Ni-poor taenite surrounded by a rim of more Ni-rich taenite.

4.1.4. Minor Minerals

Troilite and chromite occur as massive grains (5-50 μm in diameter) commonly near grain boundaries between metal and silicates. Two exceptionally large chromite grains (～200 μm and ～100 μm in diameter) are found in two different 3B particles.

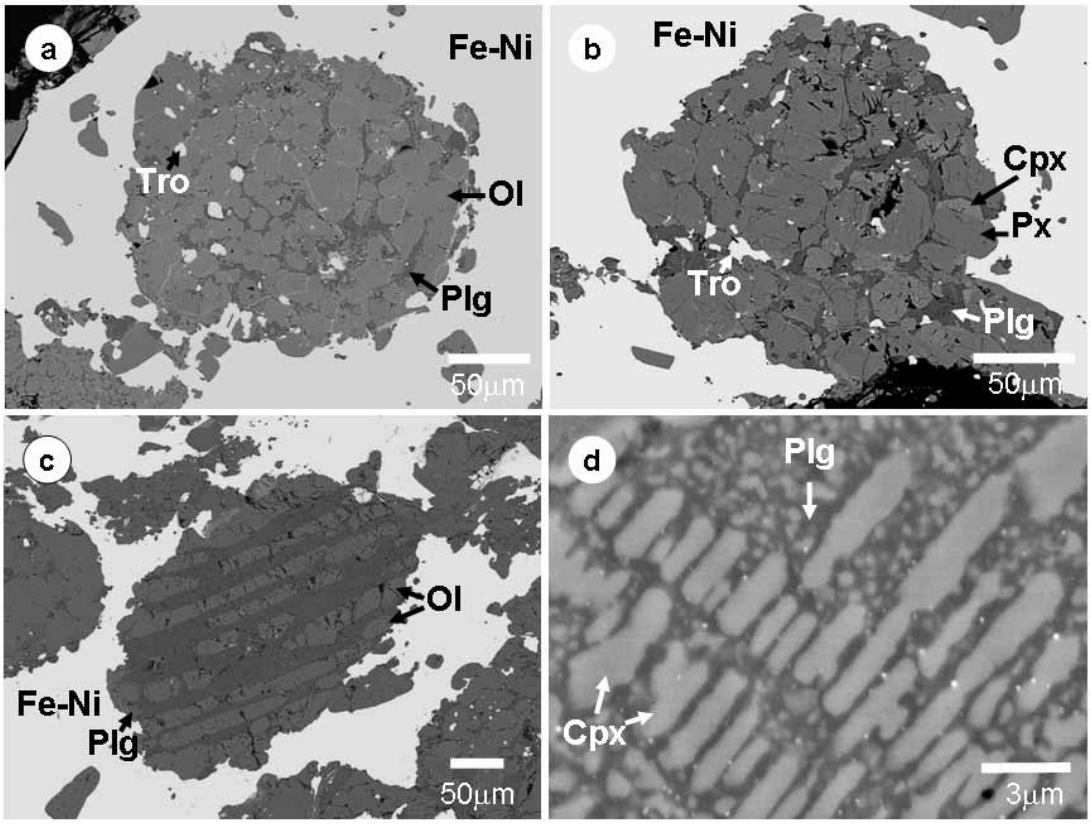

Figure 12. Backscattered electron images of chondrule-like silicate aggregates in 3B particles. (a) Porphyritic olivine type. (b) Porphyritic pyroxene type. (c) Barred olivine type. (d) High-magnification image of a portion of chondrule-like silicate aggregate, obtained using the field emission SEM, showing quenched crystallites of high-Ca pyroxene (Cpx) in plagioclase (Plg) mesostasis..Fe-Ni = Fe-Ni metal, Tro = troilite, Ol = olivine, Px = low-Ca pyroxene.

4.1.5. Shock Stage

In order to determine shock stage, we examined 14 olivine grains that are >50 μm in diameter in the 3B-1 and 3B-2 particles by the optical microscope. All the olivine grains exhibit sharp extinction, thus indicating that 3B is shock stage S1 (Stöffler et al., 1991), which means that it has no significant shock effects.

4.2. Mineral Compositions

Olivine is very homogeneous, averaging $Fa_{16.2}$ (standard deviation in Fa content = 0.6) (Table 4; Fig. 6). Olivine contains significant amounts of Mn (～0.5 wt% MnO) and trace amounts of Ca (<0.05 wt% CaO), Ti (<0.05 wt% TiO_2) and Cr (<0.1 wt% Cr_2O_3). It should be noted that these compositional characteristics are almost identical to those of the olivine in 3A.

Low-Ca pyroxene is also very homogeneous, averaging $Fs_{14.8}$ (standard deviation in Fs content = 0.8) (Fig. 7) and $Wo_{1.0}$ (Table 4; Fig. 8). It contains significant amounts of Al (～0.2 wt% Al_2O_3), Cr (～0.2 wt% Cr_2O_3), Mn (～0.5 wt% MnO). High-Ca pyroxene is also homogeneous, averaging $Fs_{7.5}$ (standard deviation in Fs content = 1.1) and $Wo_{37.3}$ (standard deviation in Wo content = 4.3), but less homogeneous than low-Ca pyroxene (Fig. 8). High-Ca pyroxene contains significant amounts of Na (～0.6 wt% Na_2O), Al (～4.0 wt% Al_2O_3), Ti (～0.7 wt% TiO_2), Cr (～1.7 wt% Cr_2O_3) and Mn (～0.4 wt% MnO). We note that, like olivine, the compositions of both low-Ca and high-Ca pyroxenes are closely similar to those in 3A.

Plagioclase is albitic (Na-rich) and variable in composition from grain to grain, ranging from An_{15} to An_{37} (Table 4; Fig. 9). The compositional characteristics are very similar to those of plagioclase in 3A.

Kamacite contains ～6.0 wt% Ni and ～0.45 wt% Co (Table 5). Taenite contains 50.1 wt% Ni and extremely low amounts of

Table 4. Electron microprobe analyses of olivine, low-Ca pyroxene, high-Ca pyroxene, plagioclase and chromite in the 3B sample (wt%).

	Olivine		Low-Ca		High-Ca		Plagioclase		Chromite	
No. of Analyses	49	(s.d.)	34	(s.d.)	10	(s.d.)	15	(s.d.)	6	(s.d.)
Na_2O	0.01	(0.01)	0.02	(0.02)	0.61	(0.14)	7.40	(1.35)	0.04	(0.02)
MgO	45.0	(0.6)	32.5	(0.4)	18.3	(1.5)	0.07	(0.13)	3.99	(1.39)
Al_2O_3	0.01	(0.02)	0.21	(0.19)	3.99	(0.60)	25.3	(2.2)	5.88	(0.24)
SiO_2	39.2	(0.4)	56.2	(0.5)	51.5	(0.5)	59.8	(4.0)	0.02	(0.02)
K_2O	0.00	(0.01)	0.00	(0.01)	0.00	(0.01)	0.22	(0.14)	0.00	(0.00)
CaO	0.03	(0.10)	0.55	(0.23)	17.2	(1.8)	6.19	(2.70)	0.00	(0.00)
TiO_2	0.04	(0.05)	0.08	(0.05)	0.67	(0.22)	0.04	(0.02)	1.42	(0.14)
Cr_2O_3	0.05	(0.07)	0.20	(0.26)	1.67	(0.13)	0.03	(0.06)	58.6	(0.6)
MnO	0.45	(0.04)	0.49	(0.06)	0.35	(0.06)	0.01	(0.01)	1.46	(0.16)
FeO	15.5	(0.6)	10.2	(0.6)	4.47	(0.71)	0.61	(0.30)	27.4	(1.6)
NiO	0.02	(0.03)	0.03	(0.06)	0.01	(0.01)	0.01	(0.02)	0.02	(0.03)
Total	100.3		100.5		98.8		99.7		98.8	
Mol%										
Fa	16.2	(0.6)	-	(-)	-	(-)	-	(-)	-	(-)
Fs	-	(-)	14.8	(0.8)	7.5	(1.1)	-	(-)	-	(-)
Wo	-	(-)	1.0	(0.4)	37.3	(4.7)	-	(-)	-	(-)
Ab	-	(-)	-	(-)	-	(-)	68.4	(10.7)	-	(-)
An	-	(-)	-	(-)	-	(-)	25.8	(11.2)	-	(-)
Or	-	(-)	-	(-)	-	(-)	1.5	(0.7)	-	(-)

s.d.: standard deviation.

Table 5. Electron microprobe analyses of kamacite, taenite and troilite in the 3B sample (wt%).

	Kamacite		Taenite		Troilite	
No. of Analyses	87	(s.d.)	18	(s.d.)	11	(s.d.)
P	0.00	(0.00)	0.00	(0.00)	0.00	(0.00)
Si	0.01	(0.02)	0.01	(0.01)	0.05	(0.02)
S	0.00	(0.00)	0.00	(0.00)	36.9	(0.2)
Cr	0.02	(0.05)	0.01	(0.01)	0.02	(0.02)
Fe	93.8	(0.7)	49.3	(1.4)	62.8	(0.6)
Ni	5.95	(0.42)	50.1	(1.5)	0.01	(0.01)
Co	0.45	(0.02)	0.07	(0.01)	0.00	(0.00)
Total	99.8		99.4		99.8	

s.d.: standard deviation.

Co (～0.07 wt%). The slight compositional variation in taenite (standard deviation in Ni content = 4.4 wt%) may be ascribed to the core-to-rim Ni zoning. Kamacite closely resembles in composition that in 3A, whereas taenite is considerably richer in Ni content than that in 3A.

Chromite contains considerable Mg (～4.0 wt% MgO), Al (～5.9 wt% Al_2O_3), appreciable Ti (～1.4 wt% TiO_2) and Mn (～1.5 wt% MgO) (Table 4). Ca-phosphate contains neither Cl nor F.

5. DISCUSSION

5.1. 3A sample

We initially assumed that this test sample is powder prepared by crushing and grinding a meteorite sample, and we tried to

determine its classification based on petrographic and mineralogical characteristics.

At the early stage of our study, we found that particles in 3A contain materials that are obviously part of chondrules. They are similar to the most common textural types of chondrules in chondrites such as PO, PP and BO. Therefore, we thought that 3A is probably powder of a chondrite. The major constituent minerals are Fe-rich olivine and pyroxene that are highly homogeneous in composition. These characteristics led us to further assume that this sample is an equilibrated ordinary chondrite that belongs to one of H, L and LL groups. Most major and minor minerals in 3A occur in equilibrated ordinary chondrites (OC). Equilibrated OC are classified as petrologic types 4-6 that have undergone significant equilibration as a result of thermal metamorphism on meteorite parent bodies. Major constituent minerals of type 4-6 OC are olivine, low-Ca pyroxene and Fe-Ni metal, and their compositions can be used as fundamental diagnostic properties to determine the classification of OC into H, L and LL.

5.1.1. Chemical Group

It is well established that olivine and low-Ca pyroxene compositions in type 4-6 OC from H, L and LL groups fall in well-defined fields in a plot of the fayalite (Fa) content versus the ferrosilite (Fs) content (e.g., Mason, 1963; Keil and Fredriksson, 1964; Sears and Axon, 1976; Afiattalab and Wasson, 1980; Rubin, 1990) (Fig. 13). Molar Fe/(Fe+Mg) ratios in both olivine and low-Ca pyroxene increase linearly with overall oxidation state of the chondrite. Our study revealed that the compositions of olivine and low-Ca pyroxene in 3A are plotted near the Fe-poor end within the H chondrite field (Fig. 13).

Minor element contents of olivines in type 4-6 OC are known to be very uniform, regardless of chemical group (e.g., Brearley and Jones, 1998). MnO contents are between 0.4 and 0.5, but TiO_2, Al_2O_3, Cr_2O_3 and CaO contents are all extremely low, <0.1 wt%. All the minor element contents of olivine in 3A are consistent with those in type 4-6 OC (Table 2).

Low-Ca pyroxenes in type 4-6 OC have <2 mol% Wo ($CaSiO_3$) contents and contain various minor elements that show significant ranges, but MnO and Cr_2O_3 contents are relatively uniform, 0.4-0.5 wt% and 0.1-0.2 wt%, respectively (e.g., Brearley and Jones, 1998). The Wo contents and the minor element contents of low-Ca pyroxene in 3A also fall in the ranges for those in type 4-6 OC.

High-Ca pyroxenes in type 4-6 OC have relatively narrow ranges of Fs content. However, like low-Ca pyroxene, mean Fs contents for each chondrite group have a tendency to increase from Fs_7 (H) to $Fs_{8.5}$ (L) to Fs_{10} (LL) (Brearley and Jones, 1998). The mean Fs content of high-Ca pyroxene in 3A ($Fs_{6.4}$) most closely fits the H group.

Metals in type 4-6 OC have been extensively studied in the past, and the relationship between their compositions and chondrite groups has been well established. Previous workers (Sears and Axon, 1975, 1976; Afiattalab and Wasson, 1980; Rubin, 1990) showed that Co contents in kamacite progressively increase, whereas Ni contents decrease from H to L to LL chondrites, and that Co and Ni contents fall in distinct ranges within each of the different groups (Fig. 14). On the other hand, Co and Ni contents in taenite also fall in different ranges, although the resolution of the ranges is not as distinct as kamacite. Both Co and Ni contents in kamacite and taenite in 3A fall in the ranges for H chondrites (Fig. 14).

Because fayalite (Fa) contents in olivine and Co contents in kamacite are excellent parameters for OC classification as shown above, Kallemeyn et al. (1989) and Rubin (1990) constructed a plot of Co content versus Fa content (Fig. 15). The plot shows the beautiful exponential relationship. H chondrites form a tight cluster at the lower left that is well separated from L and LL chondrites that form clusters at the center and the right, respectively. The 3A sample falls near the Fa-poor and Co-poor end within the H chondrites cluster (Fig. 15).

In summary, the compositional characteristics of olivine, low-Ca and high-Ca pyroxene and Fe-Ni metals in 3A are the most similar to those in equilibrated ordinary chondrites of H type among the known chondrite groups. The compositional characteristics of other minerals, including plagioclase, chromite and phosphate, are also similar to those in equilibrated H chondrites.

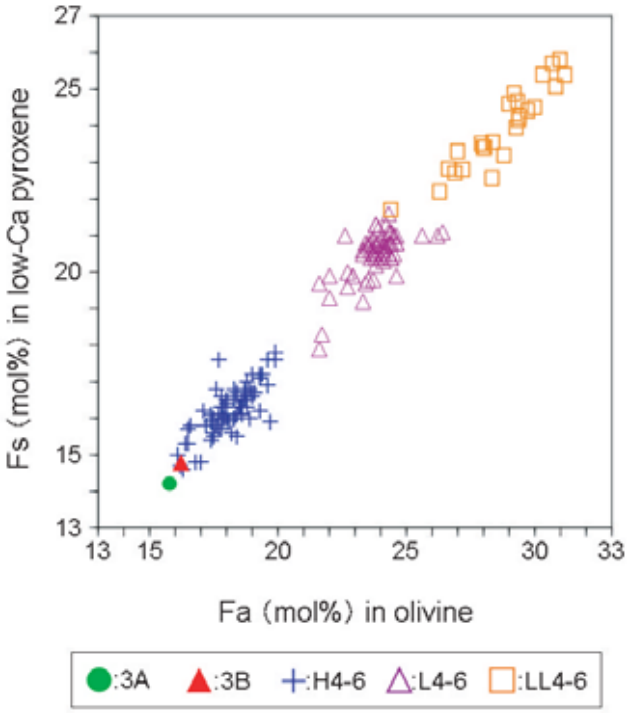

Figure 13. Fs vs Fa contents (mol%) of low-Ca pyroxene and olivine in the 3A and 3B samples and the type 4-6 ordinary chondrites.Data source of ordinary chondrites: Brearley and Jones (1998).

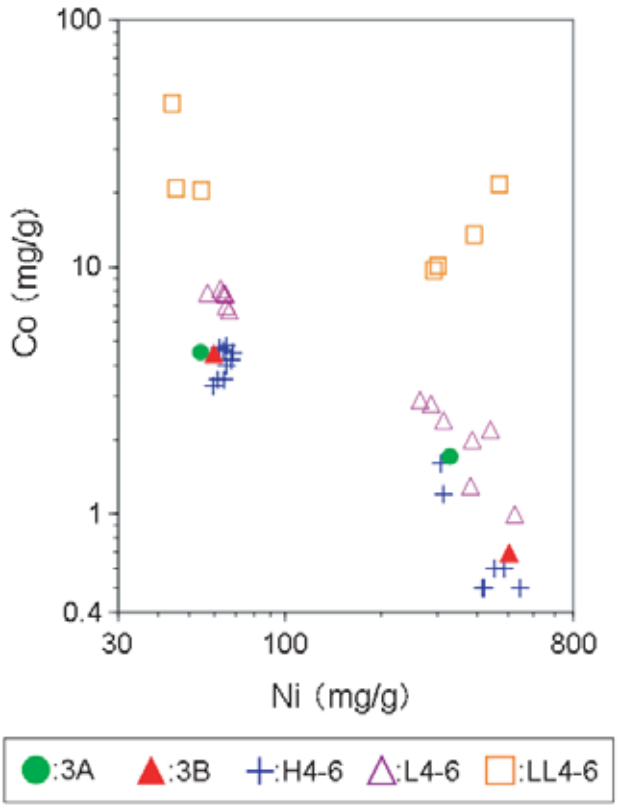

Figure 14. Co vs Ni (mg/g) diagram for kamacite and taenite in the 3A and 3B samples and the type 4-6 ordinary chondrites.Data source of ordinary chondrites: Brearley and Jones (1998).

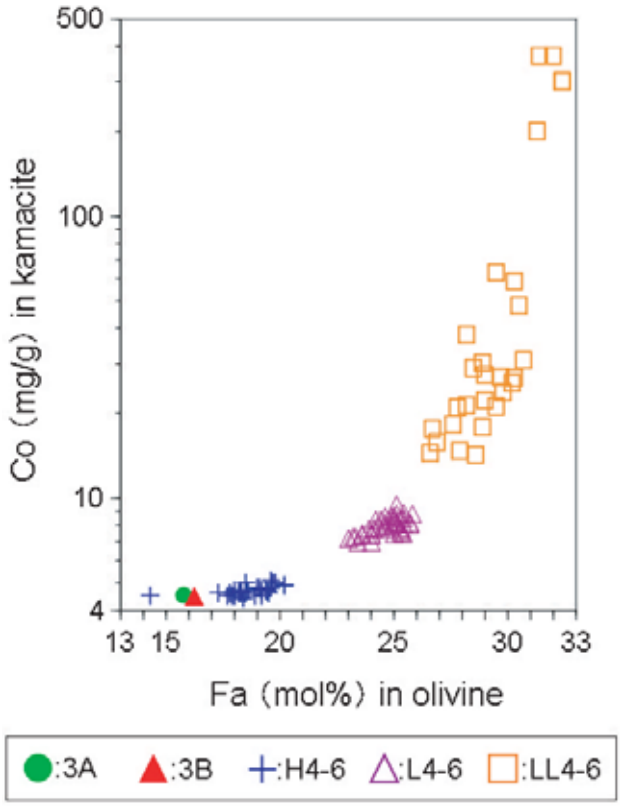

Figure 15. Co (mg/g) vs Fa (mol%) contents of kamacite and olivine in the 3A and 3B samples and the type 4-6 ordinary chondrites.Data source of ordinary chondrites: Brearley and Jones (1998).

5.1.2. Petrologic Type

Because 3A is powder consisting of small particles (<150 μm in diameter), it was difficult to determine petrologic type of its parent chondrite from petrographic characteristics. However, fine-grained olivine and pyroxene that appear to have constituted chondrite matrix are abundant in the particles, and chondrule mesostasis with fine-grained quenched crystallites are well preserved. TEM observations showed that most low-Ca pyroxene grains are clino-pyroxene and glassy grains with plagioclase composition are present. All these characteristics suggest that the parent chondrite is relatively low petrologic type, perhaps type 4.

It is known that Fa contents of olivine and Fs contents of low-Ca pyroxene within each of H, L and LL chondrite groups show slight increases as a function of petrologic type, although the changes are not so remarkable (Scott et al., 1986; Rubin, 1990; McSween and Labotka, 1993; Brearley and Jones, 1998). The increases may be due to progressive oxidation that occurred during metamorphism in the OC parent bodies (McSween and Labotke, 1993). Both olivine and low-Ca pyroxene compositions in 3A fall near the Fe-poor end within the H chondrite range (Fig. 15), which also supports our view that 3A can be classified into a relatively low petrologic type.

5.1.3. Shock Metamorphic Effects

Because we did not make regular thin sections, we could not precisely determine shock stage of 3A. Our limited observations, using a transmitted light optical microscope, show that some olivine grains exhibit weak undulatory extinction, but they are minor in abundance, which suggests that shock metamorphic effects are very minor. The dislocation-poor nature of olivine and the low degree of stacking disorder in clino-pyroxene are also consistent with the minor effects of shock metamorphism. However, we found some evidence suggesting shock effects. Plagioclase in some particles contains numerous

vesicles and micro-inclusions of Fe-Ni metal and troilite (Figs. 4a, b). The texture is similar to the vesicular, inclusion-rich plagioclase in CK chondrites (Tomeoka et al., 2001, 2005), which has been regarded as a product of recrystallization from shock-induced melts. However, because of very limited data available, it is difficult to further confirm the relationship between plagioclase in 3A and CK chondrites.

5.2. 3B sample

As in the case of 3A, we assumed that 3B has been prepared by crushing and grinding a meteorite sample and tried to determine its classification. At the beginning, however, we were puzzled with the peculiar rounded, potato-like morphology of the particles and the predominant occurrence of Fe-Ni metal (42-72 vol%) in the particles. We thought that it is difficult to produce such uniformly rounded particles simply by crushing and grinding a meteorite sample and it is also difficult to crush such a metal-rich rock to produce such small particles.

Silicate-rich portions in the 3B particles occur as aggregates that are analogous in texture to chondrules in chondrites. Some are fragments, most of which appear to have been derived from larger complete chondrules. Most of the major textural types of chondrules including PO, POP, BO, GO and PP are present. Few large fragments preserve arcuate edges with large radii of curvature. From these observations, we thought that 3B has been prepared from a chondrite, like 3A. Because of high abundance of Fe-Ni metal, we initially assumed that 3B belongs to one of the metal-rich chondrite groups such as CB, CH and CR. However, as we studied the details of mineralogy and petrology, we became to be suspicious of this assumption, since many mineralogical and petrological characteristics of 3B do not exactly fit any of the known metal-rich chondrites.

The major constituent minerals of the silicate aggregates, which we identified as chondrules, in 3B are Fe-rich olivine and pyroxene that are highly homogenous in composition. To our surprise, the compositions of both olivine and low-Ca pyroxene are almost identical to those in 3A (Tables 2 and 4). In addition, the compositions of kamacite are also indistinguishable from those in 3A (Tables 3 and 5). All these results indicate that 3B is related to equilibrated H chondrites. After knowing these results, we recognized the possibility that 3B does not necessarily represent a bulk meteorite but a fraction of a meteorite. We envisaged that the rounded 3B particles may correspond to individual metal grains contained in an H chondrite.

It is known that equilibrated H chondrites contain ～8.4 vol% Fe-Ni metal (e.g., Krot et al., 2004), which occurs as grains typically 0.1-3 mm in size, evenly distributed throughout the meteorites, in addition to globules which occur inside chondrules. Those metal grains commonly contain chondrules and chondrule fragments, bearing a close resemblance to the 3B particles. We presume that, if such chondrule-bearing metal grains are separated from the parent meteorite and ground by a mortar, such rounded (potato-like) mineral assemblages as seen in the 3B particles would be produced.

In addition to the major minerals in 3B, most of less abundant minerals, including high-Ca pyroxene, plagioclase, chromite, phosphate and taenite, also have compositions being similar to those of the counterparts in equilibrated H chondrites (e.g., Brearley and Jones, 1998). Other mineralogical and petrological characteristics in 3B such as (1) chondrule textures, (2) lamellae texture in kamacite, (3) compositional zoning in kamacite and taenite are also known to be common in equilibrated OC (Gooding and Keil, 1981; Brearley and Jones, 1998; Willis and Goldstein, 1983; Wood, 1967; Nagahara, 1979). Therefore, we conclude that 3B is probably related to equilibrated H chondrites. As discussed above (section 5.1), Fa contents of olivine and Fs contents of low-Ca pyroxene in 3B suggest that its petrologic type is relatively low.

6. SUMMARY

The general appearance and mineral abundances of the 3A and 3B sample are very different. 3A is composed of angular to irregularly shaped particles (<150 μm in diameter) that consist mainly of Fe-rich olivine, low-Ca pyroxene and lesser amounts of high-Ca pyroxene and plagioclase, whereas 3B is composed of rounded to subrounded particles (0.2-2.3 mm in diameter) that consist mainly of Fe-Ni metal and lesser amounts of Fe-rich olivine and low-Ca pyroxene. However, the results of our study revealed that most of the constituent minerals in 3A and 3B occur in common, and almost all of them have very similar

compositions that are most similar to those of the counterparts in equilibrated H ordinary chondrites. Therefore, we suggest that 3A is powder made of a silicate-rich fraction of an H chondrite sample and 3B is made of a metal-rich fraction of an H chondrite sample. 3B particles may be silicate-bearing metal grains that were separated from a disaggregated H chondrite sample. Because the compositions of olivine, low-Ca pyroxene and kamacite in 3A and 3B are very close to each other, we think it is possible that 3A and 3B have been prepared from the same meteorite. Although precise determination of petrologic type could not be made because of very small particle size, the mineralogical characteristics of 3A and 3B suggest that the petrologic type of both samples is relatively low.

Acknowledgments: We thank Mr. Y. Shibata for discussion about EPMA analyses of metals and Prof. Y. Tainosho for the use of FESEM. Electron microprobe analysis was performed at the Venture Business Laboratory, Kobe University. This work was supported by Grant-in-Aid (No. 16204042) and "The 21st Century COE Program of Origin and Evolution of Planetary Systems" of the Japan Ministry of Education, Culture, Sports, Science and Technology.

REFERENCES

Afiattalab, F. and Wasson, J.T., 1980, Composition of the metal phases in ordinary chondrites: Implications regarding classification and metamorphism, *Geochimica et Cosmochimica Acta*, **44**, 431-446.

Binzel, R.P., Rivkin, A.S., Bus, S.J., Sunshine, J.M. and Burbine, T.H., 2001, MUSES-C target asteroid (25143) 1998 SF36: A reddened ordinary chondrite, *Meteoritics and Planetary Science*, **36**, 1167-1172.

Brearley, A.J. and Jones, R.H., 1998, Chondritic meteorites, in Planetary Materials, Reviews in Mineralogy (ed. J. J. Papike) *Mineralogical Society of America*, **36**, 398.

Gooding, J.L. and Keil, K., 1981, Relative abundances of chondrule primary textural types in ordinary chondrites and their bearing on conditions of chondrule formation, *Meteoritics*, **16**, 17-43.

Kallemeyn, G.W., Rubin, A.E., Wang, D. and Wasson, J.T., 1989, Ordinary chondrites: Bulk compositions, classification, lithophile-element fractionations, and composition-petrographic type relationships, *Geochimica et Cosmochimica Acta*, **53**, 2747-2767.

Keil, K. and Fredriksson, K., 1964, The iron, magnesium, and calcium distribution in coexisting olivines and rhombic pyroxenes of chondrites, *J. Geophys. Res*., **64**, 3487-3515.

Krot, A.N., Keil, K., Goodrich, C.A. and Scott, E.R.D., 2004, Classification of Meteorites, 83-128., in Meteorites, Comets, and Planets (ed. A.M. Davis) Vol. 1 Treatise on Geochemistry (eds. H.D. Holland and K.K. Turekian), Elsevier-Pergamon, Oxford.

Lederer, S.M., Domingue, D.L., Vilas, F., Abe, M., Farnham, T.L., Jarvis, K.S., Lowry, S.C., Ohba, Y., Weissman, P.R., French, L.M., Fukai, H., Hasegawa, S., Ishiguro, M., Larson, S.M. and Takagi, Y., 2005, Physical characteristics of Hayabusa target Asteroid 25143 Itokawa, *Icarus*, **173**, 153-165.

Mason, B., 1963, Olivine composition in chondrites, *Geochimica et Cosmochimica Acta*, **27**, 1011-1023.

McSween, H.Y. Jr. and Labotka, T.C., 1993, Oxidation during metamorphism of the ordinary chondrites, *Geochimica et Cosmochimica Acta*, **57**, 1105-1114.

Nagahara, H., 1979, Petrological Study of Ni-Fe Metal in Some Ordinary Chondrites, *Mem. NIPR. Spec. Issue*., **15**, 111-122.

Rubin, A.E., 1990, Kamacite and olivine in ordinary chondrites: Intergroup and intragroup relationships, *Geochimica et Cosmochimica Acta*, **54**, 1217-1232.

Scott, E.R.D., Taylor, G.J., Keil, K., McKinely, S.G. and Wilson, I.E., 1986, Accretion, metamorphism and brecciation of ordinary chondrites: Evidence from petrologic studies of meteorites from Roosevelt Country, *Meteoritics*, **21**, 509.

Sears, D.W. and Axon, H.J., 1975, Metal of high Co content in LL chondrites, *Meteoritics*, **11**, 97-100.

Sears, D.W. and Axon, H.J., 1976, Ni and Co content of chondritic metal, *Nature*, **260**, 34-35.

Shibata, Y., 1996, Opaque minerals in Antarctic CO3 carbonaceous chondrites, Yamato-74135, -790992, -791717, -81020, -81025, -82050 and Allan Hills-77307, *Proc. NIPR symp. Antarct. Meteorites*, **9**, 79-96.

Stöffler, D., Keil, K. and Scott, E.R.D., 1991, Shock metamorphism of ordinary chondrites, *Geochimica et Cosmochimica Acta*, **55**, 3845-3867.

Tomeoka, K., Ohnishi, I. and Nakamura, N., 2001, Silicate darkening in the Kobe CK chondrite: Evidence for shock metamorphism at high temperature, *Meteoritics and Planetary Science*, **36**, 1535-1545.

Tomeoka, K., Kojima, T., Ohnishi, I., Ishii, Y. and Nakamura, N., 2005, The Kobe CK carbonaceous chondrite: Petrography, mineralogy and metamorphism, *Journal of Mineralogical and Petrological Sciences*, **100**, 116-125.

Willis, J. and Goldstein, J.I., 1983,A three-dimensional study of metal grains in equilibrated, ordinary chondrites, *Proc. Lunar Planet. Sci*., **14B**, 287-292.

Wood, J. A., 1967, Chondrites: Their metallic minerals, thermal histories, and parent planets, *Icarus*, **6**, 1-49.